Effect of Acute Intraocular Pressure Elevation on the Monkey Optic Nerve Head as Detected by Spectral Domain Optical Coherence Tomography

Nicholas G. Strouthidis,[1,2] *Brad Fortune,*[3] *Hongli Yang,*[1] *Ian A. Sigal,*[4] *and Claude F. Burgoyne*[1]

Purpose. To determine whether acutely elevated IOP alters optic nerve head (ONH) structural parameters characterized in vivo using spectral domain optical coherence tomography (SD-OCT).

Methods. Five rhesus macaques were tested under isoflurane anesthesia. SD-OCT images of the ONH of both eyes were acquired 30 minutes after IOP was stabilized to 10 mm Hg and 60 minutes after stabilization to 45 mm Hg. The internal limiting membrane, Bruch's membrane/retinal pigment epithelium, neural canal opening (NCO), and anterior lamina cribrosa surface (ALCS) were delineated using custom software. Differences in SD-OCT structural parameters between the two IOP levels were assessed using generalized estimating equations. In six eyes of three animals, images were acquired after 10 minutes and 30 minutes of IOP stabilization to 10 mm Hg (control experiment).

Results. Acute IOP elevation resulted in a reduction in prelaminar tissue thickness (mean, −47 μm; SD, 25 μm; P = 0.002), rim volume (−0.05 mm^3, 0.02 mm^3; P = 0.002), rim width (−30 μm, 7 μm; P = 0.002), and in an increase in NCO depth (38 μm, 15 μm; P = 0.002). An increase in ALCS depth was significant relative to peripheral Bruch's membrane (48 μm, 24 μm; P = 0.002) but not relative to the NCO. No significant parameter changes were detected in the control eyes.

Conclusions. Surface compliance changes in the normal monkey ONH primarily reflect prelaminar and peripapillary deformation. SD-OCT compliance testing will further our understanding of the effects of IOP on the ONH and help improve and validate numerical models of ONH biomechanics. (*Invest Ophthalmol Vis Sci.* 2011;52: 9431–9437) DOI:10.1167/iovs.11-7922

From the [1]Optic Nerve Head Research Laboratory and [3]Discoveries in Sight Laboratories, Devers Eye Institute, Legacy Health, Portland, Oregon; [2]Glaucoma Research Unit, Moorfields Eye Hospital, London, United Kingdom; and [4]Laboratory of Ocular Biomechanics, University of Pittsburgh, Pittsburgh, Pennsylvania.

Supported by National Institutes of Health Grant R01-EY11610, Legacy Good Samaritan Foundation, Heidelberg Engineering (NGS), Sears Medical Trust, and a Royal College of Ophthalmologists/Pfizer Fellowship (NGS).

Submitted for publication May 22, 2011; revised September 20, 2011; accepted October 20, 2011.

Disclosure: **N.G. Strouthidis**, Heidelberg Engineering (F, R); **B. Fortune**, Heidelberg Engineering (F); **H. Yang**, None; **I.A. Sigal**, None; **C.F. Burgoyne**, Heidelberg Engineering (F, R)

Corresponding author: Claude F. Burgoyne, Optic Nerve Head Research Laboratory, Devers Eye Institute, Legacy Health, 1225 NE 2nd Avenue, Portland, OR 97208-3950; cfburgoyne@deverseye.org.

Although the clinical entity of glaucoma is well recognized as an optic neuropathy with its characteristic structural changes of the optic disc, associated loss of retinal nerve fiber layer (RNFL), and specific pattern of visual field loss, the pathophysiology of retinal ganglion cell (RGC) loss that underlies these observations continues to be an area of debate. Given that IOP-lowering strategies (whether pharmacologic, surgical, or laser) are, to date, the only proven methods by which to slow the progression of glaucoma,[1–3] it is reasonable to assume that IOP plays a role in the pathophysiology of glaucoma. Furthermore, this treatment strategy holds true for glaucoma subjects with statistically normal levels of IOP (normal tension glaucoma),[2,4] suggesting that IOP plays an important role in the development of glaucoma, regardless of the absolute level of IOP.

The biomechanical paradigm is based on the premise that IOP acts as a mechanical load resulting in stress and strain of the tissues in and around the optic nerve head, in particular the lamina cribrosa and the peripapillary sclera.[5] This paradigm postulates that IOP-related biomechanical stresses and strains act as key instigators of glaucomatous damage in the optic nerve head (ONH). Further, the paradigm proposes that the biomechanical effects of IOP result in changes to the ONH microstructure that underpin susceptibility to vascular insult.[5] Understanding the biomechanical behavior of the ONH can be aided by the application of imaging techniques to monitor ONH "compliance " while load (IOP) is varied.

The compliance of the normal ONH in response to an acute elevation of IOP has been studied by a series of investigators using a number of techniques, including X-ray photography of cadaveric nonhuman primate eyes with fine platinum wires inserted into the peripapillary sclera and optic disc,[6] laser Doppler velocimetry of normal human autopsy eyes,[7] conventional histology of human eyes,[8] two-dimensional (2D)[9,10] and three-dimensional (3D) histomorphometric reconstructions of postmortem normal monkey eyes,[11] and various imaging modalities in vivo in normal monkey eyes[12,13] with subsequent application of numerical models.[14,15] The studies, conducted in vivo using imaging technology, were all consistent in their findings (to a greater or lesser degree) of a posterior movement of the optic disc surface in response to an acute elevation of IOP. Studies that were performed either ex vivo or with histologic specimens suggested that the surface changes detectable in vivo by imaging may reflect changes to the underlying load bearing connective tissues of the ONH, in particular the lamina cribrosa, but, until recently, imaging technologies did not allow examination of these deeper structures in vivo.

To date, the biomechanics of the ONH have only been explored ex vivo, augmented by modeling strategies such as finite element modeling.[16–18] This is a computational tool that enables prediction of how a biological tissue with complex architecture and material properties will respond to different

magnitudes of load. This technique is limited by the accuracy of the inputs, specifically knowledge of the geometry and material properties of the tissues examined. With the commercial introduction of high-speed, high-resolution spectral domain optical coherence tomography (SD-OCT), it has become feasible to detect structures deep to the surface of the optic disc cup, including the prelaminar tissue, the lamina cribrosa, and, in some eyes, the peripapillary sclera.[19–22] Compliance testing using SD-OCT, if successful, should allow us to test the hypothesis that the surface changes seen with acute elevation of IOP using other imaging modalities underpin changes to deeper connective tissues. Such "deep " in vivo compliance testing may also serve to verify or refute the observations made ex vivo and to further advance computational studies of ONH biomechanics.[14,15,23]

We have recently described a series of structural parameters derived from 3D SD-OCT ONH volumes that were used to detect longitudinal changes in the neuroretinal rim width (RW) and rim volume (RV), prelaminar tissue thickness, and anterior lamina cribrosa surface at the earliest stages of the monkey experimental glaucoma model.[24] We have also previously published a study examining the effect of acute IOP elevation on peripapillary nerve fiber layer thickness as detected by SD-OCT and some preliminary observations regarding changes at the ONH in both eyes of five normal rhesus macaques.[25] In the present study, we applied our strategy for delineation and parameterization of the ONH structure to that acute IOP imaging data set to investigate the effect of acutely elevated IOP on ONH structures detected in vivo using SD-OCT.

Methods

Animal Selection

The local Institutional Animal Care and Use Committee (Legacy Health) approved this study, and all animals were treated in accordance with the ARVO Statement for the Use of Animals in Ophthalmic and Vision Research. Two young (younger than 3 years), two young adult (age range, 3–8 years), and one adult (older than 8 years) rhesus macaque monkeys (*Macaca mulatta*) were included in this study (Table 1). The mean (range) age of subject animals included was 5.6 (1–10) years, and the mean (range) weight was 5.0 (2.7–7.2) kg.

Anesthesia and IOP Control

The testing protocol is a variant of protocols that have been previously described in detail.[25,26] In brief, all animals were induced using ketamine (15 mg/kg, by intramuscular injection) and midazolam (0.2 mg/kg, by intramuscular injection) and were anesthetized through an endotracheal tube using an inhaled mixture of 100% oxygen and isoflurane gas (1%–2%; typically 1.25%) for the duration of the imaging session. Blood pressure was monitored at 10-minute intervals (NIBP system 7100; Advanced Medical Instruments, Inc., Broken Arrow, OK), and a mean arterial pressure (MAP) >75 mm Hg was maintained. We administered an intravenous bolus of lactated Ringer's (10 mL/kg/h) solution if MAP was <70 mm Hg, and then discontinued testing (with recovery of the subject) if the MAP did not respond to IV fluid administration.

We controlled IOP by inserting cannulae into both anterior chambers through the temporal peripheral corneas and then connecting the cannulae to an adjustable height reservoir of sterile balanced salt solution (BSS; Alcon Laboratories, Inc., Forth Worth, TX) through polyurethane tubing. The height of the reservoir could be adjusted by 5-mm Hg increments.

Table 1. Characteristics of Subject Animals Included in the Study

ID	Age (y)	Weight (kg)	SD-OCT Scan Pattern	Experimental Protocol
23534	10	4.0	80 radial B-scans	Acute IOP + control
21808	7	6.0	80 radial B-scans	Acute IOP + control
21152	8	7.2	80 radial B-scans	Acute IOP + control
25340	2	5.4	48 radial B-scans	Acute IOP
25904	1	2.7	48 radial B-scans	Acute IOP

Note that alternate B-scans were delineated for the 80 radial B-scan pattern volumes (i.e., 40 B-scans per volume), whereas all B-scans were delineated for the 48 radial B-scan volumes (i.e., 48 B-scans per volume). All animals were included in the acute IOP experimental protocol whereby two SD-OCT volumes were acquired after 30 minutes at IOP 10 mm Hg (first volume) and after a combined 30 minutes at IOP 30 mm Hg and 60 minutes at IOP 45 mm Hg (second volume). Three animals also had a single volume acquired after 10 minutes at IOP 10 mm Hg, which was compared with the volume acquired after 30 minutes at IOP 10 mm Hg (control experimental protocol).

ONH Imaging

The imaging protocol has been described in our previous publication.[25] Briefly, both pupils were dilated using 1 drop each of tropicamide (0.5%) and phenylephrine (2.5%), and a clear, plano-powered, rigid, gas-permeable contact lens was placed on each eye.

All ONH imaging was performed using a commercially available SD-OCT device (Spectralis; Heidelberg Engineering GmbH, Heidelberg, Germany). We acquired 80 radial B-scan images (15° location; 768 A-scans per B-scan), centered on the ONH, from both eyes of three animals and 48 radial B-scan images from the other two animals. The device's eye-tracking facility was turned on during image acquisition to enable B-scan acquisition repetition ($n = 9$) and sweep averaging in real time to reduce speckle noise. For each eye, the scans were not referenced to the "baseline " image to prevent any distortion of the images caused by image processing rather than by acute IOP elevation. However, within each volume, the individual B-scans were registered to each other along the z-axis by post hoc processing based on the native SD-OCT (Spectralis; Heidelberg Engineering GmbH) algorithm for this function.

Testing Protocol

At the start of the imaging session, IOP in both eyes was adjusted to 10 mm Hg, and SD-OCT scans were acquired after a 30-minute period of stabilization at this IOP. In six eyes of three animals, SD-OCT images were also acquired after 10 minutes of IOP stabilization at 10 mm Hg. IOP was then raised to 30 mm Hg in both eyes for 30 minutes and to 45 mm Hg in both eyes for 60 minutes, after which the SD-OCT scans were repeated. SD-OCT data were compared between the IOP 45-mm Hg condition (60 minutes of IOP at 45 mm Hg but 90 minutes of total IOP elevation above 10 mm Hg) and the baseline 10-mm Hg condition at 30 minutes. Scans acquired after 10 minutes at IOP 10 mm Hg were matched against those obtained at 30 minutes at IOP 10 mm Hg; this served as a control experiment to evaluate interscan variability in the absence of any IOP change. Of note, image acquisition during acute IOP elevation to 45 mm Hg was unaffected by the presence of corneal edema, which was minimal or negligible throughout the testing procedure.

Delineation and Parameterization of SD-OCT Volumes

The SD-OCT delineation methodology used in this study has been described in detail elsewhere.[24,27] Raw SD-OCT data from each volume were exported into Multiview, a custom-built, 3D visualization and delineation software (based on the Visualization Toolkit, VTK, Clifton Park, NY). Three observers, masked to each IOP condition, manually delineated pertinent features within alternating B-scans of the 80 radial B-scan volumes (i.e., 40 B-scans per 80 radial B-scan volume; six eyes of three animals) and in every B-scan of the 48 radial B-scan volumes (four eyes of two animals). In each case, the first delineated B-scan was at the vertical 0° location, and delineation proceeded in a clockwise fashion

TABLE 2. Mean (SD) for Parameters Generated in the Acute IOP Experimental Protocol

Parameter	Condition (10 eyes total) 10/30	45/60	Comparison *P*
RNFLT, μm	122 (3.5)	120 (4.1)	0.0230
RNFLV, mm^3	0.28 (0.09)	0.28 (0.09)	0.0001
RW, μm	**282 (39.2)**	**252 (34.3)**	**<0.0001**
RV, mm^3	**0.30 (0.06)**	**0.26 (0.05)**	**<0.0001**
NCO depth, μm	**60 (15.0)**	**98 (24.7)**	**<0.0001**
NCO area, mm^2	1.25 (0.19)	1.25 (0.22)	1.0000
ALCS depth$_{NCO}$, μm	179 (28.4)	189 (37.0)	0.0190
ALCS depth$_{BM}$, μm	**241 (29.1)**	**290 (44.0)**	**<0.0001**
PLTT, μm	**371 (76.9)**	**324 (58.3)**	**<0.0001**

10/30 condition refers to parameters derived from an image acquisition after 30 minutes at IOP 10 mm Hg; 45/60 condition refers to parameters derived from an image acquisition after 60 minutes at IOP 45 mm Hg. Pairwise comparisons were performed using the generalized estimating equation, $P < 0.005$. Significant parameters are in bold.

through each of the successive B-scans. The features delineated were as follows: internal limiting membrane (ILM), posterior surface of the retinal nerve fiber layer (RNFL), posterior surface of the Bruch's membrane/retinal pigment epithelium complex (BM/RPE), neural canal opening (NCO; located on either side of the neural canal at the innermost termination of the BM/RPE),[27] border tissue of Elschnig (located on either side of the neural canal at the innermost termination of the choroidal signal),[22,28] and anterior lamina cribrosa surface (ALCS). (An example of each of these delineation categories is provided in Supplementary Fig. S1, http://www.iovs.org/lookup/suppl/doi:10.1167/iovs.11-7922/-/DCSupplemental).

Our strategy for identifying the ALCS was based on our previous direct comparisons between SD-OCT B-scans and matched histologic sections obtained from the same normal monkey eye.[22] It is important to point out that the signal from the ALCS may be discontinuous in regions with pronounced shadowing caused by overlying retinal vessels. The observer could, therefore, use any number of marks, at his or her discretion, to delineate the ALCS.

Our parameterization strategy has been described elsewhere.[24] We defined two reference planes—a primary reference plane anchored at the NCO and a secondary, peripheral, reference plane anchored at 1500 μm external to the NCO centroid, along the RPE/BM complex. We generated the following parameters: mean depth of NCO (height of NCO relative to the secondary reference plane), mean RNFL thickness (RNFLT), RNFL volume (RNFLV), NCO area, neuroretinal mean rim width (RW) and neuroretinal rim volume (RV). All parameters generated are global and thus generated as mean values derived from the 40 or 48 B-scans delineated in each SD-OCT volume. The exceptions to this were volume measurements (RNFLV and RV), which are calculated by interpolation of surfaces between adjacent B-scans in each SD-OCT volume, and NCO area, which was derived from the area of a best-fitting ellipse.[24]

ALCS delineations were "weighted " according to their distance from the NCO centroid to achieve proportionality (i.e., peripheral laminar marks represent a wider arc—a greater portion of the wedge represented by each radial B-scan—than central laminar marks). In our previous description of this parameter, we advocated using regions of ALCS delineation that were common, or shared, to each of the volumes for a particular eye to restrict the number of spurious delineations, in a process we called point filtration.[24] For the present study, there were considerably fewer scans available for each eye (two) compared with the previous study (four); therefore, point filtration would likely have resulted in the loss of potentially useful data. Hence, we elected to include all delineated ALCS points for each volume. Furthermore, we have previously demonstrated that, at least in terms of experimental glaucoma, there appears to be no effect of either time or treatment (experimental glaucoma) on the area of ALCS detectable by SD-OCT.[24]

Using the weighted ALCS points, prelaminar tissue thickness (PLTT) and ALCS depth were calculated. ALCS depth was determined relative to the NCO reference plane (ALCS depth$_{NCO}$) and to the peripheral BM/RPE reference plane (ALCS depth$_{BM}$). Methods for quantifying the three parameters related to the ALCS delineations are illustrated in Supplementary Fig. S2, http://www.iovs.org/lookup/suppl/doi:10.1167/iovs.11-7922/-/DCSupplemental.

Statistical Analysis

All differences between the SD-OCT parameters at the two different IOP conditions (IOP 45 mm Hg after 60 minutes vs. IOP 10 mm Hg after 30 minutes for the acute IOP elevation experiment and IOP 10 mm Hg after 30 minutes vs. IOP 10 mm Hg after 10 minutes for the control IOP experiment) were calculated. All differences ($n = 10$) between the two IOP conditions were assessed using the generalized estimating equations to account for the correlation between both eyes of each animal. To correct for multiple comparisons,[29] we established a cutoff of $P < 0.005$ (based on the fact that we examined approximately 10 SD-OCT parameters ($0.05/10 = 0.005$, thus using a conservative correction essentially identical with a Bonferroni correction to maintain a family-wise type 1 error rate near 0.05). All statistical analyses were performed using commercial software (Prism, version 4.0 [GraphPad Software, Inc, San Diego, CA]), Excel [Microsoft Corporation, Redmond, WA], or R [R Foundation for Statistical Computing, Vienna, Austria]).

RESULTS

Significant structural parameter changes ($P < 0.005$) between IOP 10 mm Hg/30 minutes and IOP 45 mm Hg/60 minutes (Table 2) were observed for neuroretinal rim measurements (RW and RV, both decreasing), RNFLV (decreasing), PLTT (decreasing), ALCS depth$_{BM.}$(increasing), and NCO depth (increasing). There were no significant changes in structural parameters generated from the volumes evaluated in the control experiment (IOP 10 mm Hg/10 minutes compared with IOP 10 mm Hg/30 minutes; Table 3). Table 4 shows the change in each parameter for each eye compared between IOP 10 mm Hg/30 minutes and IOP 45 mm Hg/60 minutes. Table 5 shows the change in each parameter for each of the six eyes included in the control experiment.

Marked decreases in RW (expressed as percentage of baseline value, percentage SD; −11%, 2%), RV (−15%, 5%), and

TABLE 3. Mean (Standard Deviation) for Parameters Generated in the Control Experimental Protocol

Parameter	Condition (6 eyes total) 10/10	10/30	Comparison *P*
RNFLT, μm	121 (3.7)	123 (4.1)	0.0410
RNFLV, mm^3	0.28 (0.01)	0.29 (0.01)	0.0000
RW, μm	304 (32.0)	304 (31.3)	0.4800
RV, mm^3	0.32 (0.06)	0.32 (0.06)	0.0460
NCO depth, μm	56 (9.3)	57 (10.5)	0.0920
NCO area, mm	1.11 (0.04)	1.12 (0.03)	0.0250
ALCS depth$_{NCO}$, μm	171 (28.8)	168 (22.8)	0.2300
ALCS depth$_{BM}$, μm	229 (37.7)	228 (30.0)	0.7800
PLTT, μm	416 (76.5)	414 (68.4)	0.6700

10/10 condition refers to parameters derived from an image acquisition after 10 minutes at IOP 10 mm Hg; 10/30 condition refers to parameters derived from an image acquisition after 30 minutes at IOP 10 mm Hg. Pairwise comparisons were performed using the generalized estimating equation, $P < 0.005$.

Table 4. Changes in Each Parameter Value for Individual Eyes When Increasing IOP from 10 mm Hg/30 Minutes to 45 mm Hg/60 Minutes

ID	Eye	RNFLT (μm)	RNFLV (mm^3)	RW (μm)	RV (mm^3)	NCO Depth (μm)	NCO Area (mm^2)	ALCS $Depth_{NCO}$ (μm)	ALCS $Depth_{BM}$ (μm)	PLTT (μm)
21152	OD	−2	0.00	−33	−0.05	53	−0.02	−7	45	−61
21152	OS	−4	−0.01	−33	−0.04	51	−0.01	8	57	−46
21808	OD	−1	0.00	−34	−0.07	68	−0.02	40	111	−93
21808	OS	−1	−0.01	−37	−0.08	41	−0.04	5	50	−74
23534	OD	0	0.00	−38	−0.05	31	−0.02	0	32	−46
23534	OS	−3	−0.01	−36	−0.05	31	0.00	9	41	−52
25340	OD	1	0.00	−23	−0.03	20	0.02	6	26	−23
25340	OS	1	0.00	−22	−0.03	19	0.03	21	40	−42
25904	OD	−5	−0.01	−20	−0.04	33	0.03	11	40	−8
25904	OS	−4	−0.01	−25	−0.03	35	0.03	7	42	−24
Mean	—	−2	−0.004	−30	−0.05	38	0.00	10	48	−47
SD	—	2	0.005	7	0.02	15	0.02	13	24	25

PLTT (−12%, 5%) were observed, as were considerable increases in NCO depth (65%, 25%) and ALCS $depth_{BM}$ (20%, 8%). The amount of change observed in RNFLT, RNFLV, and NCO_{area} with elevated IOP was in each case negligible, amounting to a mean of 2% or less in either direction, which was equivalent to what had been observed for those parameters in the control experiment. Although a higher percentage change was detected for ALCS $depth_{NCO}$ with IOP elevation (5%, 6%), this change was within the interscan variability observed in the control experiment (−1%, 8%).

Figure 1 illustrates the relationship between the change in NCO depth and the change in prelaminar tissue thickness (left) and the change in RV (right) for the 10 acute IOP elevation eyes and the six control experiment eyes. In both cases, there was a clear association between the change in each parameter and the magnitude of NCO depth change ($R^2 = 0.49$ for change in prelaminar tissue thickness, $R^2 = 0.41$ for change in RV for the 10 eyes with acute IOP elevation). Images obtained from the eye with the most profound changes associated with acute elevation of IOP (right eye of animal 21808) are shown in Figure 2. The delineated structures at 10 mm Hg/30 minutes (Fig. 2A) and at IOP 45 mm Hg/60 minutes (Fig. 2B) are overlaid using the NCO reference plane (Fig. 2C) and using the secondary peripheral Bruch's membrane reference plane (Fig. 2D). An obvious posterior movement of the ILM is seen using the NCO reference plane, whereas the posterior movement of the ALCS is clearly present but less striking. When the secondary reference plane is used, the posterior movement of both the ILM and the ALCS is increased, and the posterior movement of Bruch's membrane is also seen. When examining individual eye change, only two eyes demonstrated a substantial increase in ALCS depth relative to NCO (40 μm observed for animal 21808 OD, as illustrated in Fig. 2, and 21 μm observed for animal 25340 OS). In both cases, the increase in ALCS $depth_{NCO}$ exceeded the maximal change observed for that parameter in the control group (19 μm.)

Discussion

The principal findings of this study may be summarized as follows: acute IOP elevation in the normal monkey eye resulted in significant reductions in neuroretinal rim parameters (RW and RV), prelaminar tissue thickness, and significant increases in the depth of the neural canal opening (NCO depth) and the depth of the anterior lamina cribrosa surface relative to peripheral Bruch's membrane (ALCS $depth_{BM}$). An increase in anterior lamina cribrosa surface depth relative to the NCO (ALCS $depth_{NCO}$) was detectable in some eyes.

This study has expanded on our previous work, first using digitized photographs[30] and subsequently using confocal scanning laser ophthalmoscopic images.[26] These studies identified that acute elevation of IOP results in reversible deformation of the normal ONH surface. The present study has capitalized on the ability of SD-OCT to capture structures deep to the ONH surface, thereby indicating the underlying mechanism behind surface compliance changes.

Throughout our series of in vivo compliance experiments in monkey eyes, our ongoing hypothesis has been that changes in the surface of the optic disc will reflect changes to deeper load-bearing structures, chiefly the lamina cribrosa and the peripapillary sclera. Postmortem studies, performed both in human and in monkey eyes, have indicated that the lamina cribrosa and the scleral canal wall deform after acute IOP elevation.[8–10,31] We initially explored the effect of acute IOP elevation on monkey ONH connective tissues using 2D histomorphometry by comparing a series of eyes perfusion-fixed at IOP of 10 mm Hg with eyes that had been immersion-fixed (IOP of 0 mm Hg).[10] In this first study, we observed that the lamina was thinner and more anterior, and the scleral canal diameter was larger in the IOP 10-mm Hg eyes. These observations suggested that, with acute IOP elevations at a low native IOP, the scleral canal expands, resulting in a tauter, thinner, more anteriorly placed lamina. Subsequently, we per-

Table 5. Changes in Each Parameter Value for Individual Eyes during the Control Experiment When Acquiring Images at IOP 10 mm Hg/10 Minutes and at IOP 10 mm Hg/30 Minutes

ID	Eye	RNFLT (μm)	RNFLV (mm^3)	RW (μm)	RV (mm^3)	NCO Depth (μm)	NCO Area (mm^2)	ALCS $Depth_{NCO}$ (μm)	ALCS $Depth_{BM}$ (μm)	PLTT (μm)
21152	OD	4	0	1	0	0	0	1	2	−10
21152	OS	6	0	3	0	0	0	−13	−14	−3
21808	OD	1	0	3	0	5	0	−17	−13	5
21808	OS	2	0	1	0	1	0	19	21	−15
23534	OD	1	0	−5	0	7	0	1	9	5
23534	OS	2	0	1	0	−2	0	−9	−11	10
Mean	—	3	0	1	0	2	0	−3	−1	−1
SD	—	1.9	0.0	2.9	0.0	3.4	0.0	13.1	14.3	9.8

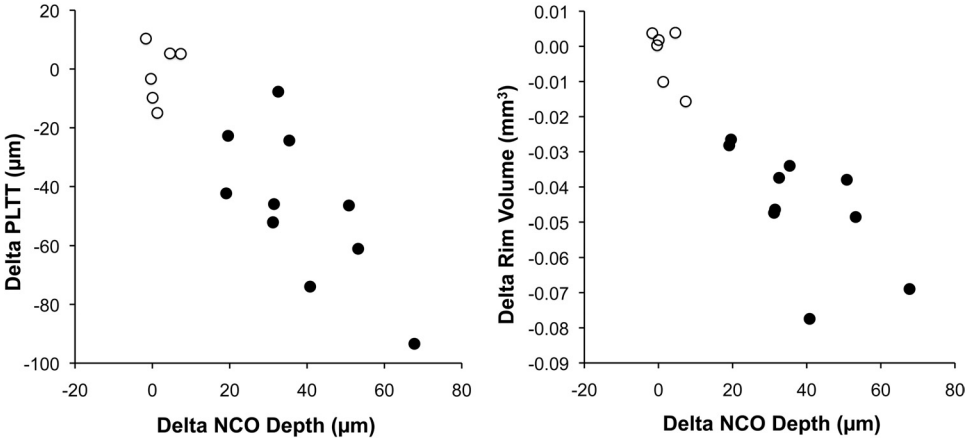

FIGURE 1. Scatter plots demonstrating the relationship between the change in NCO depth relative to a peripheral Bruch's membrane reference plane (x axes) and the change in PLTT (*left*) and RV (*right*). ○, Control experiment eyes; ●, acute IOP elevation eyes.

formed 2D histomorphometry in normal young adult monkeys perfusion fixed at 10 mm Hg in one eye and 30 or 45 mm Hg in the fellow eye.[9] In that study we demonstrated a posterior laminar deformation of 10 to 23 μm in the eyes with high IOP compared with their contralateral fellow eyes. Most recently, we have inferred the effects of acute IOP elevation by comparing postmortem 3D histomorphometric reconstruction of ONH in 12 monkeys with normal eyes whose IOP was fixed during perfusion in one eye at 30 or 45 mm Hg and in the fellow eye at 10 mm Hg.[11] In that study, we observed minimal to modest regional stretching, thinning, and deformation of the lamina cribrosa and peripapillary sclera. However, laminar deformation was minimal and was not only posterior but was also anterior in some cases (presumed to be caused by tautening of the lamina, driven by expansion of the scleral canal opening).[14,23]

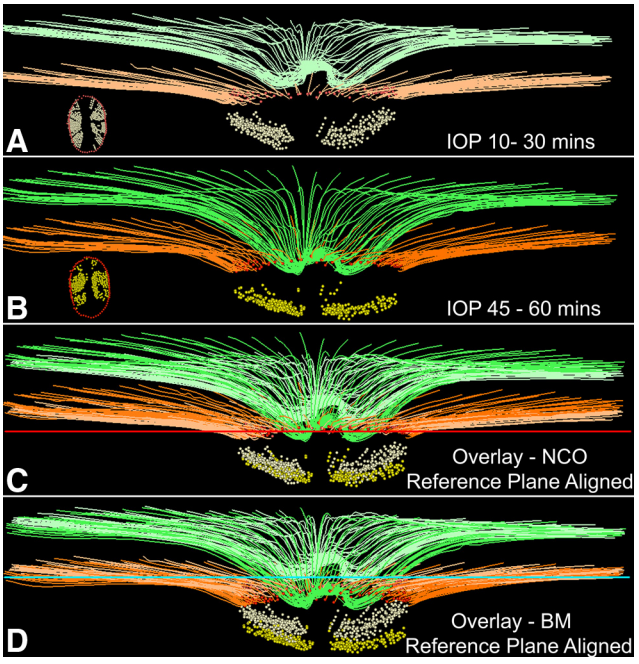

FIGURE 2. Example (animal 21808) of the SD-OCT changes observed with acute IOP elevation in a normal monkey eye. (**A**) Delineated structures at an IOP of 10 mm Hg sustained for 30 minutes. (**B**) Same structures at an IOP of 45 mm Hg after 60 minutes. (**A**, **B**, *insets*) En face views of the delineated NCO points and the ALCS points. (**C**) Delineated SD-OCT volumes have been overlaid, anchored to the NCO reference plane (*red horizontal line*). (**D**) Overlaid delineated volumes are anchored to the reference plane through the peripheral BM (*turquoise horizontal line*). Note that posterior movement of ALCS is present in (**C**), and this movement increases in (**D**), along with movement of the BM. No adjustments to z-axis magnification have been made to these images. Structures shown are ILM (*green*), BM (*orange*), NCO (*red points*), and ALCS (*yellow points*). To differentiate the structures in the overlaid images, the colors at 10 mm Hg/30 minutes have been washed out.

Overall, in the present study, changes in ALCS depth were detectable but appeared to be greater when considered relative to peripheral Bruch's membrane rather than to the NCO. This observation may be linked to the finding that significant posterior movement of the NCO relative to peripheral Bruch's membrane was also observed. In our previous study, in which we reported compliance testing in normal monkey eyes using confocal scanning laser ophthalmoscopy images,[26] we found that increasing the scan angle from 15° to 20° was often associated with an increase in surface compliance. We interpreted this phenomenon as reflecting involvement of the peripapillary sclera in the posterior deformation associated with acute IOP elevation. Given that SD-OCT was unable to capture the scleral canal opening or peripapillary sclera, we cannot be certain of the precise anatomic changes underpinning these findings.

Two eyes (animal 21808 OD, animal 25340 OS) also demonstrated substantial increases in ALCS depth$_{NCO}$, suggesting that in some eyes deformation of the ALCS is not driven solely by changes to peripapillary structures. It was not immediately apparent why these eyes should have behaved differently. One hypothesis regarding ONH compliance is that age plays a role, with young eyes expected to demonstrate increased compliance compared with aged eyes. Animal 21808 was a young adult and clearly demonstrated increased compliance compared with the older adult (animal 23534, aged 10 years) included in the study but also compared to the two younger animals (aged <3 years). Indeed there does not appear to be any clear age-related trend, with similar ALCS depth change occurring in both the young and the adult eyes, although this occurred with the caveat that only 10 eyes were available for comparison. We hypothesized that the response of the load-bearing connective tissues of the ONH (lamina cribrosa and peripapillary sclera) to acute IOP elevation will vary from subject to subject and perhaps between individual eyes in the same subject (as observed in this small study) because of variability in the material properties (themselves influenced by age and geometric properties) of the tissues under force. Further compliance testing in a larger number of monkey eyes, with a wider age range, and across the spectrum of the experimental glaucomatous process, is already under way in our laboratory.

Agoumi et al.[32] found that significant prelaminar tissue displacement but not laminar displacement was detectable by SD-OCT in vivo in 36 human subjects (including glaucoma subjects, age-matched controls, and young controls) in whom IOP was transiently elevated using an ophthalmodynamometer. The apparent similarity in results occurred despite some important methodological differences with our study. Because our study was performed in nonhuman primates, we were able to accurately and sustainably titrate IOP elevation by manometric control, whereas using an ophthalmodynamometer achieved an average estimated IOP increase of 10 mm Hg that was only sustained for the duration of the imaging session (approximately 2 minutes). Furthermore, we generated parameters using 40 or 48 radial B-scans; in the human study, only the best four matching radial B-scans from a 12-radial B-scan pattern were used. Despite these important methodological differences, the close similarity in findings between the two studies suggests that the changes observed with acute IOP elevation are consistent and likely to be generalizable. Agoumi et al.[32] used only one reference plane based on a line connecting Bruch's membrane opening points (equivalent to our primary NCO-based reference plane) and thus, unlike us, did not look for changes in lamina depth relative to the periphery.

Interestingly, a single NCO-based reference plane was also used in a recent report of ex vivo SD-OCT compliance testing using porcine eyes.[33] In contrast to both our study and the SD-OCT study performed in vivo in human eyes,[32] prelaminar tissue and lamina cribrosa cross-sectional areas within a central B-scan both significantly decreased with incremental IOP elevation. Furthermore, multivariate regression indicated that the IOP-dependent increase in the size of the cup could be explained primarily by changes in the position and cross-sectional area of the lamina cribrosa. Our own results suggest that in most cases, increases in cup (although not directly measured) are driven by a reduction in PLTT and by posterior displacement of the NCO (perhaps indirectly reflecting deformation of the peripapillary sclera). It is possible that a proportion of the posterior lamina displacement noted ex vivo in porcine eyes might have been driven by posterior displacement of the NCO/peripapillary scleral deformation, which might have been detected had a peripheral reference plane also been adopted, as in our study. Given that the lamina is more anteriorly placed within the pig ONH than in the human or monkey ONH, more of the thickness of the lamina could be captured, though it should be noted that the measurements were in two dimensions only and were not necessarily comparable to those of the present study. The apparent reduction in laminar area, which is independent of reference plane, suggested that laminar deformation plays a major role in ONH compliance in the pig eye. The apparent increased laminar deformation seen in the pig eye compared with the monkey eye may simply reflect the aforementioned differences in measurement. Accepting this major caveat, it is possible that the lamina is highly compliant in the pig eye or indeed that the observed changes might be a consequence of "stiffer " peripapillary sclera in the pig eye. This latter hypothesis might have been confirmed if significant scleral canal expansion was detectable in the monkey eye but not the pig eye[10] had it been possible to detect the deeper scleral tissues in either animal by SD-OCT. Fortunately, this is likely to be possible with 1000-nm wave source imaging or enhanced depth imaging (either at 870 nm or 1000 nm). The dynamic interaction between lamina and sclera is central to the understanding of ONH biomechanics. Capture of the deeper scleral tissues represents a major hurdle because in vivo measurements of scleral canal expansion will be needed to effectively refine and validate finite element models of ONH biomechanics.[34,35]

Agoumi et al.[32] assumed that thinning of the prelaminar tissue was a consequence of compression of the ILM and the prelaminar tissue. Numerical models, however, have suggested that acute increases in IOP would result in thinning of the prelaminar tissues because of lateral displacement, without compression.[36] The volume of prelaminar tissue may, therefore, remain unchanged with acutely elevated IOP, and the apparent thinning or compression simply reflects a redistribution of the prelaminar tissues. These changes may also be influenced by conformational alterations in adjacent structures, such as the peripapillary sclera, which was not directly measurable by SD-OCT in this study. It is likely that the increased depth penetration afforded by enhanced depth imaging or 1000-nm wave source SD-OCT, or both, may allow improved visualization of the most posterior recesses of the neural canal. If an expansion of the deeper canal is detectable, then it is feasible that the resultant increased "volume " space may allow for prelaminar and rim tissue redistribution.

This study supports the use of SD-OCT to detect in vivo changes in ONH parameters after acute elevation in IOP. There is, therefore, potential to use this technology to characterize in vivo biomechanics of the ONH in both monkey and human eyes for the first time and to further inform and validate numerical models. Such acute IOP ONH compliance testing may be of important clinical relevance because it will help differentiate permanent structural changes (assumed to be due to tissue loss or remodeling) from reversible changes. If in vivo ONH biomechanical behavior can be linked to distinct patterns of functional damage, this opens the possibility of SD-OCT–assisted compliance testing becoming a component of future risk profiling in patients with, or at risk for, glaucoma.

Acknowledgments

The authors thank Shaban Demirel for assistance with statistics in R.

References

1. Migdal C, Gregory W, Hitchings R. Long-term functional outcome after early surgery compared with laser and medicine in open-angle glaucoma. *Ophthalmology.* 1994;101:1651–1656.
2. Heijl A, Leske MC, Bengtsson B, Hyman L, Hussein M. Reduction of intraocular pressure and glaucoma progression: results from the Early Manifest Glaucoma Trial. *Arch Ophthalmol.* 2002;120:1268–1279.
3. Kass MA, Heuer DK, Higginbotham EJM, et al. The Ocular Hypertension Treatment Study: a randomized trial determines that topical ocular hypotensive medication delays or prevents the onset of primary open-angle glaucoma. *Arch Ophthalmol.* 2002;120:701–713.
4. Collaborative Normal-Tension Glaucoma Study Group. Comparison of glaucomatous progression between untreated patients with normal-tension glaucoma and patients with therapeutically reduced intraocular pressures. *Am J Ophthalmol.* 1998;126:487–497.
5. Burgoyne CF, Downs JC, Bellezza AJ, Suh JK, Hart RT. The optic nerve head as a biomechanical structure: a new paradigm for understanding the role of IOP-related stress and strain in the pathophysiology of glaucomatous optic nerve head damage. *Prog Retin Eye Res.* 2005;24:39–73.
6. Levy NS, Crapps EE. Displacement of optic nerve head in response to short-term intraocular pressure elevation in human eyes. *Arch Ophthalmol.* 1984;102:782–786.
7. Zeimer RC, Ogura Y. The relation between glaucomatous damage and optic nerve head mechanical compliance. *Arch Ophthalmol.* 1989;107:1232–1234.
8. Yan DB, Coloma FM, Metheetrairut A, Trope GE, Heathcote JG, Ethier CR. Deformation of the lamina cribrosa by elevated intraocular pressure. *Br J Ophthalmol.* 1994;78:643–648.
9. Bellezza AJ, Rintalan CJ, Thompson HW, Downs JC, Hart RT, Burgoyne CF. Deformation of the lamina cribrosa and anterior

scleral canal wall in early experimental glaucoma. *Invest Ophthalmol Vis Sci.* 2003;44:623–637.

10. Bellezza AJ, Rintalan CJ, Thompson HW, Downs JC, Hart RT, Burgoyne CF. Anterior scleral canal geometry in pressurised (IOP 10) and non-pressurised (IOP 10) normal monkey eyes. *Br J Ophthalmol*. 2003;87:1284–1290.
11. Yang H, Downs JC, Sigal IA, Roberts MD, Thompson H, Burgoyne CF. Deformation of the normal monkey optic nerve head connective tissue after acute IOP elevation within 3-D histomorphometric reconstructions. *Invest Ophthalmol Vis Sci.* 2009;50:5785–5799.
12. Coleman AL, Quigley HA, Vitale S, Dunkelberger G. Displacement of the optic nerve head by acute changes in intraocular pressure in monkey eyes. *Ophthalmology.* 1991;98:35–40.
13. Quigley HA, Pease ME. Change in the optic disc and nerve fiber layer estimated with the glaucoma-scope in monkey eyes. *J Glaucoma.* 1996;5:106–116.
14. Sigal IA, Yang H, Roberts MD, Burgoyne CF, Downs JC. IOP-induced lamina cribrosa displacement and scleral canal expansion: an analysis of factor interactions using parameterized eye-specific models. *Invest Ophthalmol Vis Sci.* 2011;52:1896–1907.
15. Roberts MD, Liang Y, Sigal IA, et al. Correlation between local stress and strain and lamina cribrosa connective tissue volume fraction in normal monkey eyes. *Invest Ophthalmol Vis Sci.* 2010; 51:295–307.
16. Sigal IA, Flanagan JG, Tertinegg I, Ethier CR. Finite element modeling of optic nerve head biomechanics. *Invest Ophthalmol Vis Sci.* 2004;45:4378–4387.
17. Girard MJ, Downs JC, Bottlang M, Burgoyne CF, Suh JK. Peripapillary and posterior scleral mechanics, part II: experimental and inverse finite element characterization. *J Biomech Eng.* 2009;131: 051012.
18. Downs JC, Roberts MD, Burgoyne CF, Hart RT. Multiscale finite element modeling of the lamina cribrosa microarchitecture in the eye. *Conf Proc IEEE Eng Med Biol Soc.* 2009;2009:4277–4280.
19. Kagemann L, Ishikawa H, Wollstein G, et al. Ultrahigh-resolution spectral domain optical coherence tomography imaging of the lamina cribrosa. *Ophthalmic Surg Lasers Imaging.* 2008;39:S126–S131.
20. Srinivasan VJ, Adler DC, Chen Y, et al. Ultrahigh-speed optical coherence tomography for three-dimensional and en face imaging of the retina and optic nerve head. *Invest Ophthalmol Vis Sci.* 2008;49:5103–5110.
21. Inoue R, Hangai M, Kotera Y, et al. Three-dimensional high-speed optical coherence tomography imaging of lamina cribrosa in glaucoma. *Ophthalmology.* 2009;116:214–222.
22. Strouthidis NG, Grimm J, Williams GA, Cull GA, Wilson DJ, Burgoyne CF. A comparison of optic nerve head morphology viewed by spectral domain optical coherence tomography and by serial histology. *Invest Ophthalmol Vis Sci.* 2010;51:1464–1474.
23. Sigal IA, Flanagan JG, Tertinegg I, Ethier CR. 3D morphometry of the human optic nerve head. *Exp Eye Res.* 2010;90:70–80.
24. Strouthidis NG, Fortune B, Yang H, Sigal IA, Burgoyne CF. Longitudinal change detected by spectral domain optical coherence tomography in the optic nerve head and peripapillary retina in experimental glaucoma. *Invest Ophthalmol Vis Sci.* 2011;52: 1206–1219.
25. Fortune B, Yang H, Strouthidis NG, et al. The effect of acute intraocular pressure elevation on peripapillary retinal thickness, retinal nerve fiber layer thickness, and retardance. *Invest Ophthalmol Vis Sci.* 2009;50:4719–4726.
26. Heickell AG, Bellezza AJ, Thompson HW, Burgoyne CF. Optic disc surface compliance testing using confocal scanning laser tomography in the normal monkey eye. *J Glaucoma.* 2001;10:369–382.
27. Strouthidis NG, Yang H, Fortune B, Downs JC, Burgoyne CF. Detection of optic nerve head neural canal opening within histomorphometric and spectral domain optical coherence tomography data sets. *Invest Ophthalmol Vis Sci.* 2009;50:214–223.
28. Strouthidis NG, Yang H, Reynaud JF, et al. Comparison of clinical and spectral domain optical coherence tomography optic disc margin anatomy. *Invest Ophthalmol Vis Sci.* 2009;50:4709–4718.
29. Yan J. geepack: yet another package for generalized estimating equations. *R-News.* 2002;2/3:12–14.
30. Burgoyne CF, Quigley HA, Thompson HW, Vitale S, Varma R. Measurement of optic disc compliance by digitized image analysis in the normal monkey eye. *Ophthalmology.* 1995;102:1790–1799.
31. Albon J, Purslow PP, Karwatowski WS, Easty DL. Age related compliance of the lamina cribrosa in human eyes. *Br J Ophthalmol.* 2000;84:318–323.
32. Agoumi Y, Sharpe GP, Hutchison DM, Nicolela MT, Artes PH, Chauhan BC. Laminar and prelaminar tissue displacement during intraocular pressure elevation in glaucoma patients and healthy controls. *Ophthalmology.* 2011;118:52–59.
33. Fatehee N, Yu PK, Morgan WH, Cringle SJ, Yu DY. The impact of acutely elevated intraocular pressure on the porcine optic nerve head. *Invest Ophthalmol Vis Sci.* 2011;52:6192–6198.
34. Sigal IA, Ethier CR. Biomechanics of the optic nerve head. *Exp Eye Res.* 2009;88:799–807.
35. Sigal IA, Flanagan JG, Ethier CR. Factors influencing optic nerve head biomechanics. *Invest Ophthalmol Vis Sci.* 2005;46:4189–4199.
36. Sigal IA, Flanagan JG, Tertinegg I, Ethier CR. Modeling individual-specific human optic nerve head biomechanic, I: IOP-induced deformations and influence of geometry. *Biomech Model Mechanobiol.* 2009;8:85–98.